Supplementary Materials: Something You Need Might Be under Your Feet: Molecular Magnetism of Heavy Kramers Lanthanide Hydrated Chlorides and Their Complexes with Polydentate Terpy Ligand

Svetlana P. Petrosyants, Konstantin A. Babeshkin, Andrey B. Ilyukhin, Pavel S. Koroteev * and Nikolay N. Efimov

N.S. Kurnakov Institute of General and Inorganic Chemistry, Russian Academy of Sciences, Leninsky Prosp. 31, 119991 Moscow, Russia; petros@igic.ras.ru (S.P.P.); bkonstantan@yandex.ru (K.A.B.); ilyukhin@gmail.com (A.B.I.); nnefimov@yandex.ru (N.N.E.)

* Correspondence: pskoroteev@list.ru

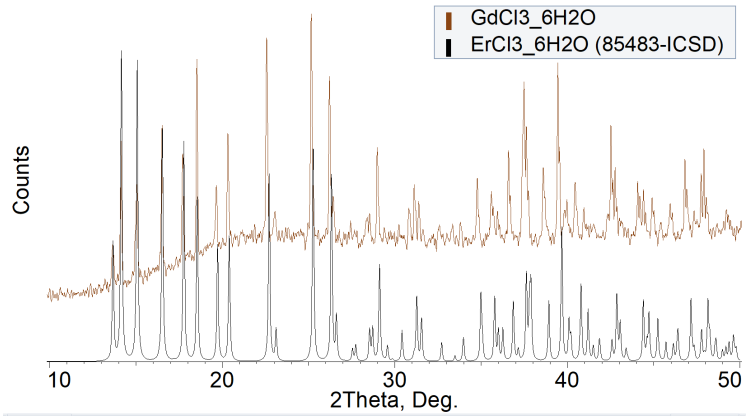

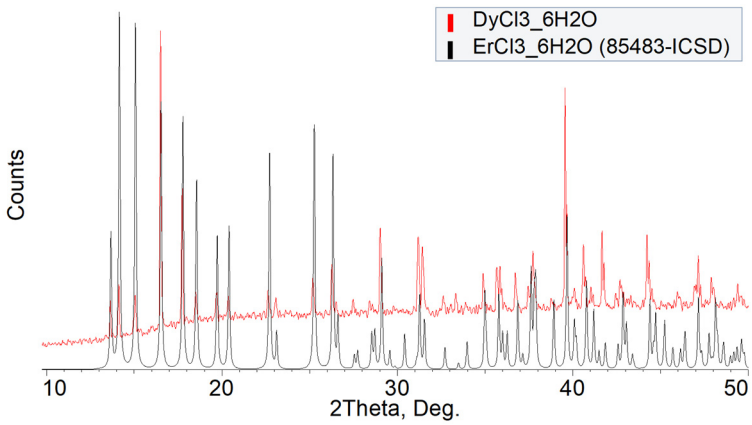

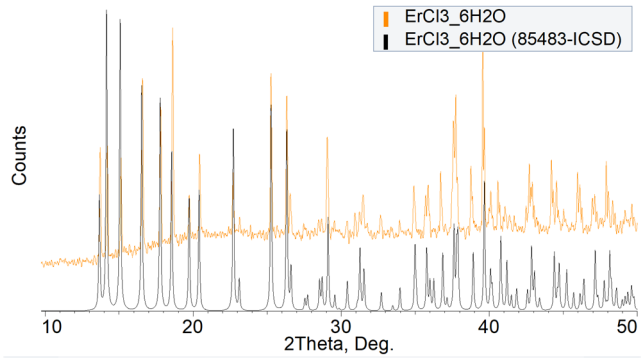

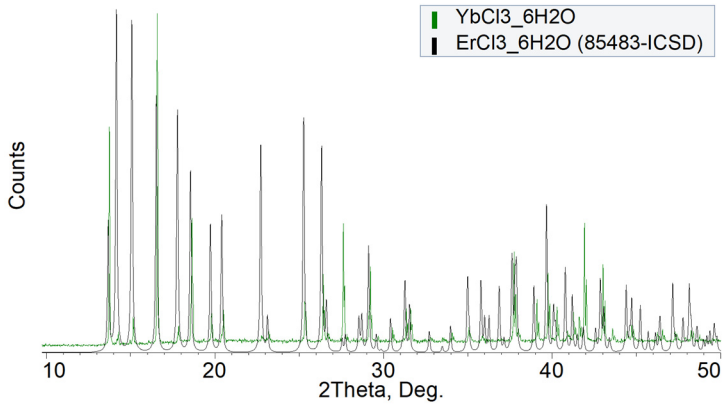

Figure S1. Powder XRD patterns of complexes **1Gd**-**1Yb** in comparison with the calculated powder XRD pattern of $ErCl_3 \cdot 6H_2O$.

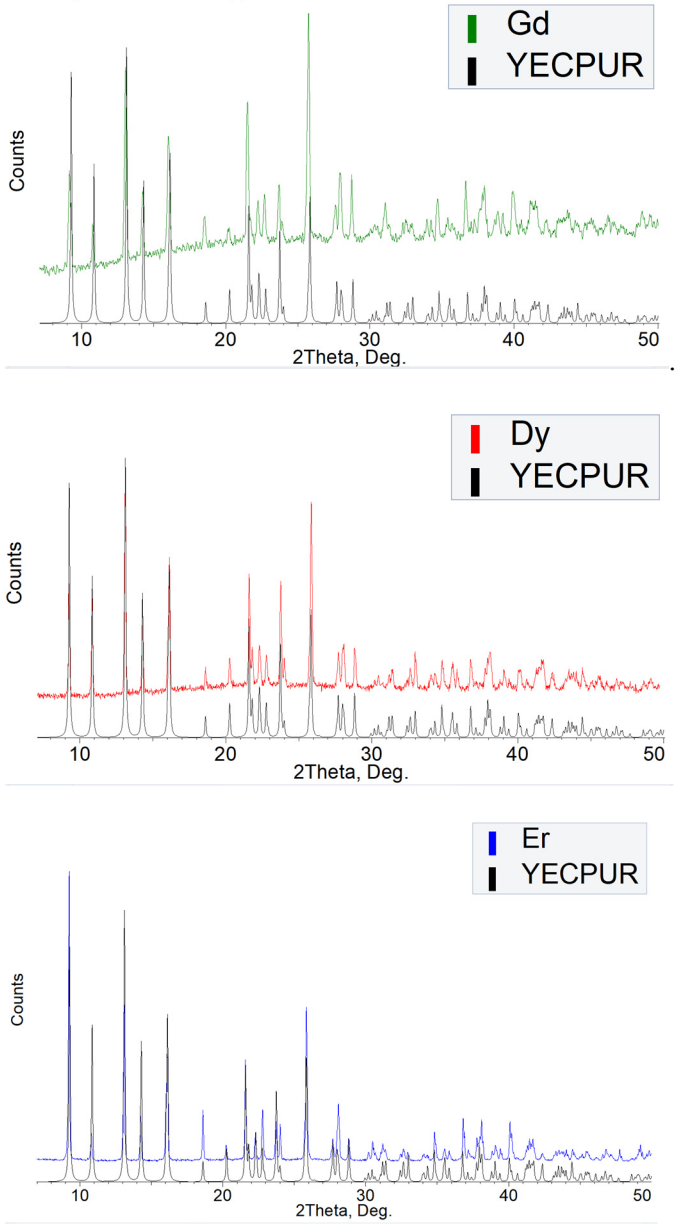

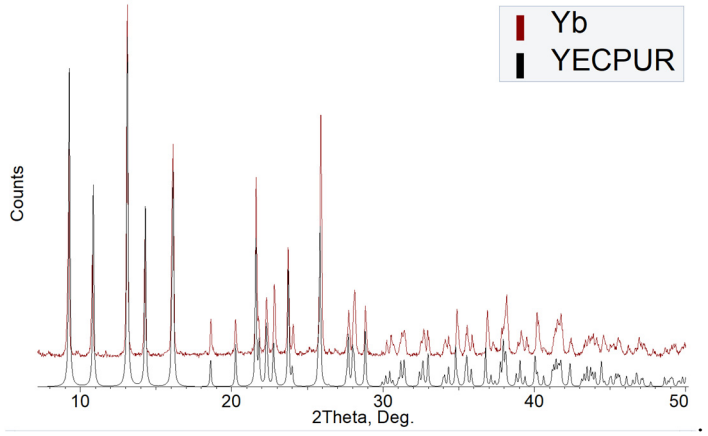

Figure S2. Powder XRD patterns of complexes **2Gd-2Yb** in comparison with the calculated powder XRD pattern of $[Y(H_2O)_4(terpy)Cl]Cl_2{\cdot}3H_2O$.

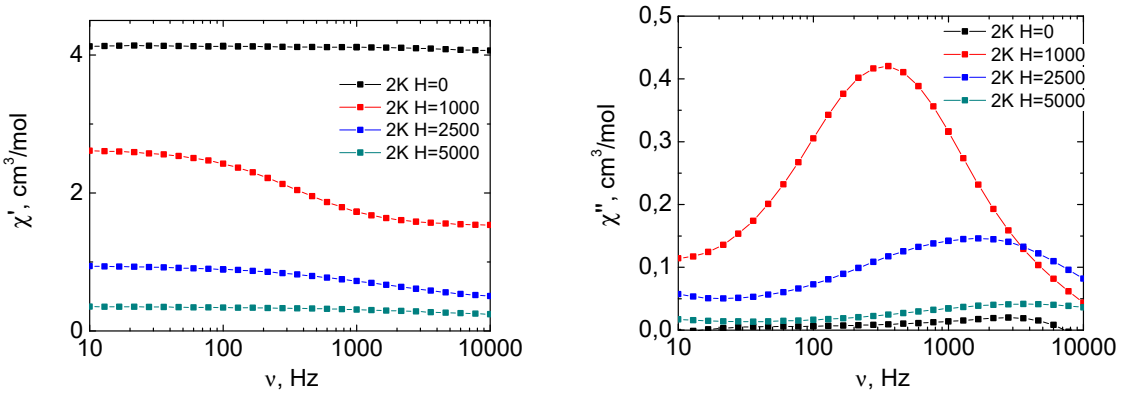

Figure S3. Frequency dependencies of in-phase, χ' (**left**) and out-of-phase, χ'' (**right**) components of dynamic magnetic susceptibility for complex **1Dy** at T = 2 K under various dc magnetic fields. Solid lines are visual guides.

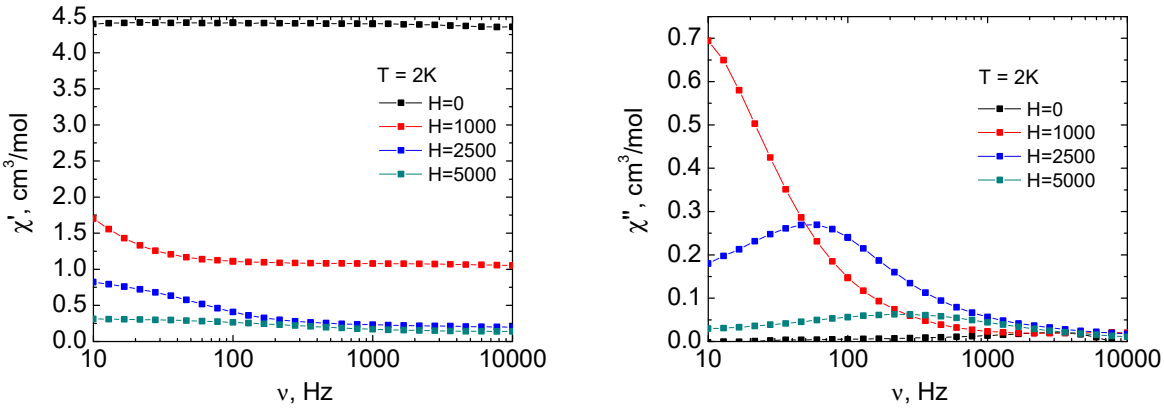

Figure S4. Frequency dependencies of in-phase, χ' (**left**) and out-of-phase, χ'' (**right**) components of dynamic magnetic susceptibility for complex **1Er** at T = 2 K under various dc magnetic fields. Solid lines are visual guides.

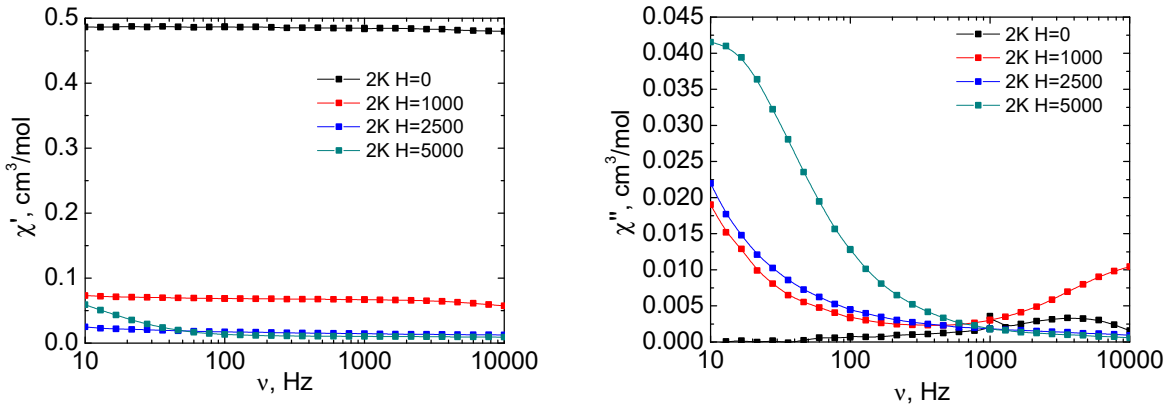

Figure S5. Frequency dependencies of in-phase, χ' (left) and out-of-phase, χ'' (right) components of dynamic magnetic susceptibility for complex **1Yb** at T = 2 K under various dc magnetic fields. Solid lines are visual guides.

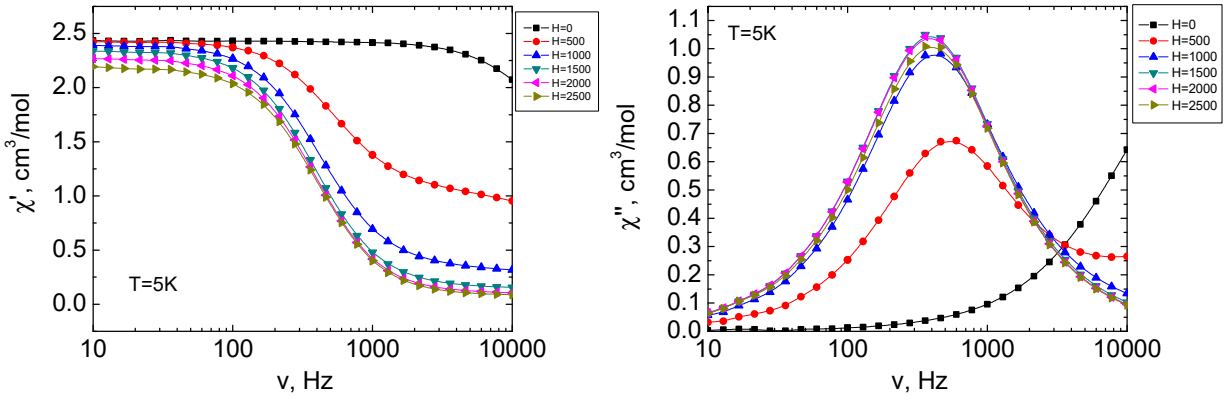

Figure S6. Frequency dependencies of in-phase, χ' (**left**) and out-of-phase, χ'' (**right**) components of dynamic magnetic susceptibility for complex **2Dy** at T = 2 K under various dc magnetic fields. Solid lines are visual guides.

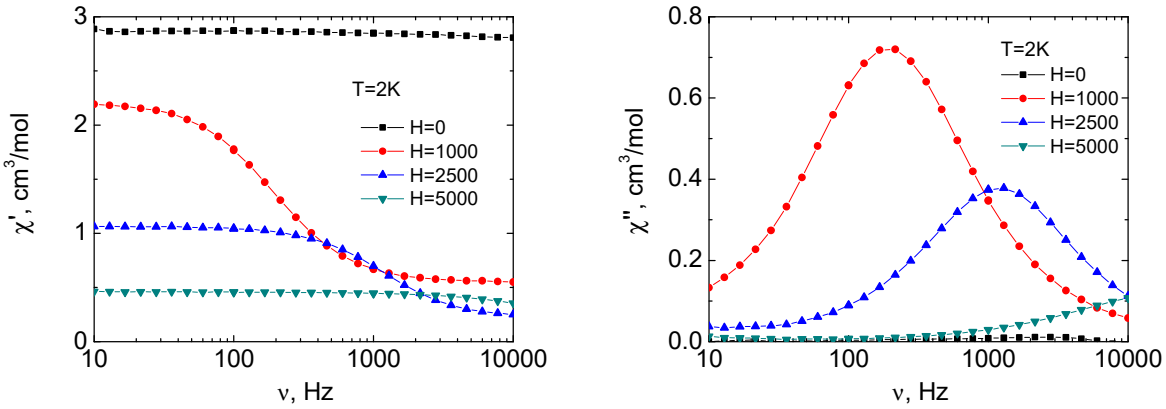

Figure S7. Frequency dependencies of in-phase, χ' (**left**) and out-of-phase, χ'' (**right**) components of dynamic magnetic susceptibility for complex **2Er** at T = 2 K under various dc magnetic fields. Solid lines are visual guides.

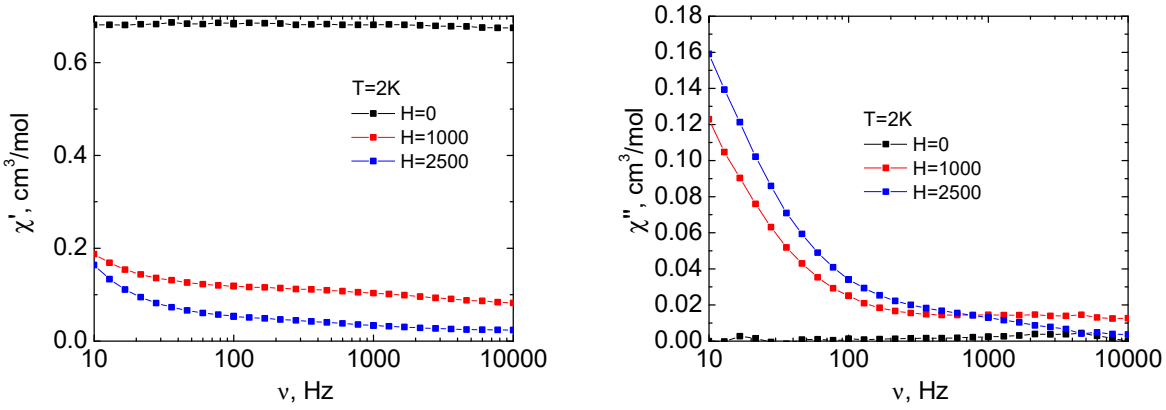

Figure S8. Frequency dependencies of in-phase, χ' (**left**) and out-of-phase, χ'' (**right**) components of dynamic magnetic susceptibility for complex **2Yb** at T = 2 K under various dc magnetic fields. Solid lines are visual guides.

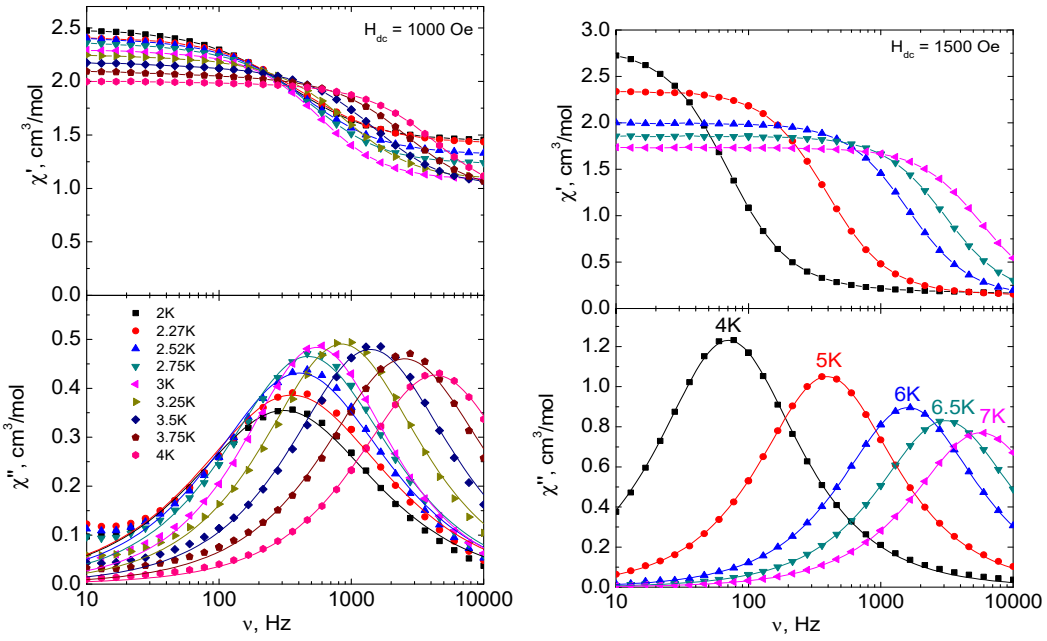

Figure S9. Frequency dependencies of the in-phase, χ' (**top**) and out-of-phase, χ'' (**bottom**) components of the ac susceptibility for **1Dy** in 1000 Oe dc-field (**left**) and for **2Dy** in 1500 Oe dc-field (**right**). Solid lines were fitted using the generalized Debye model.

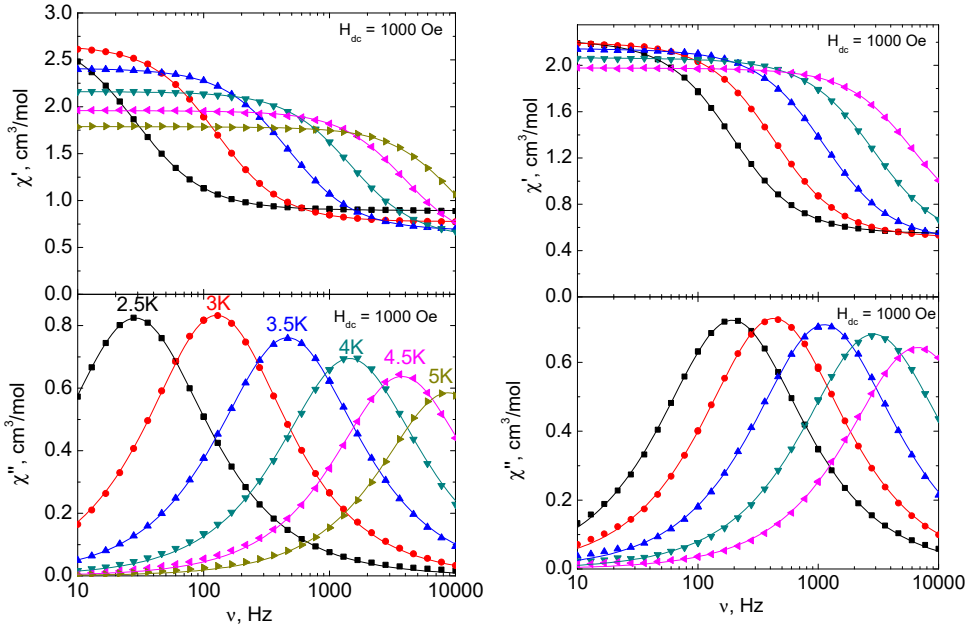

Figure S10. Frequency dependencies of the in-phase, χ' (**top**) and out-of-phase, χ'' (**bottom**) components of the ac susceptibility between 2.5 and 5 K for **1Er** (**left**) and between 2 and 4 K for **2Er** (**right**) in 1000 Oe dc-field. Solid lines were fitted using the generalized Debye model.

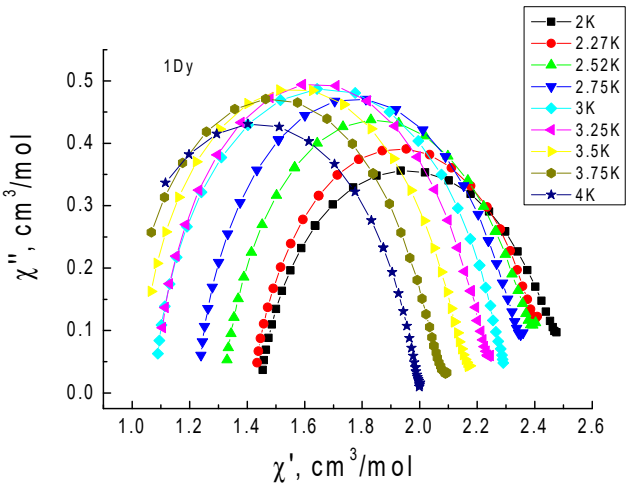

Figure S11. The Cole-Cole plot for **1Dy**.

Table S1. The values of the α parameters obtained by approximating the dependences χ'(ν) and χ''(ν) for the **1Dy** complex by the generalized Debye model.

Temperature, K	χ'(ν)	χ''(ν)
2	0.1800	0.2045
2.27	0.1681	0.217
2.52	0.1494	0.1759
2.75	0.1264	0.1437
3	0.0744	0.0798
3.25	0.1132	0.1143
3.5	0.1275	0.1192
3.75	0.1529	0.1332
4	0.1303	0.1182

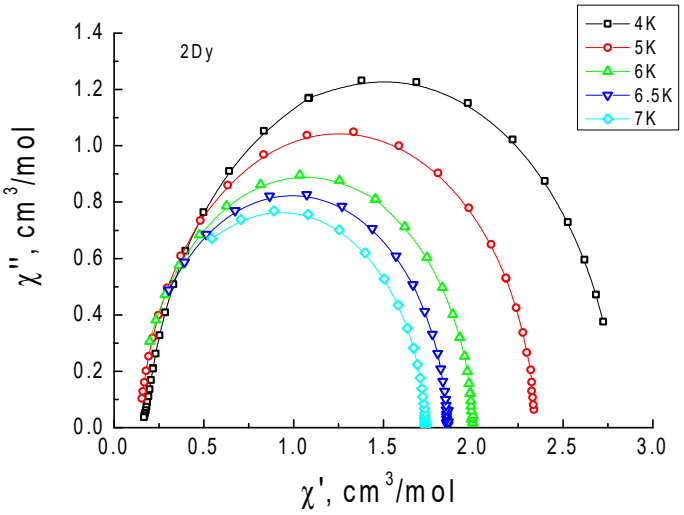

Figure S12. The Cole-Cole plot for **2Dy**.

Table S2. The values of the α parameters obtained by approximating the dependences $\chi'(\nu)$ and $\chi''(\nu)$ for the **2Dy** complex by the generalized Debye model.

Temperature, K	$\chi'(\nu)$	$\chi''(\nu)$
4	0.0415	0.0397
5	0.0258	0.0284
6	0.0250	0.0257
6.5	0.0269	0.0259
7	0.0300	0.0281

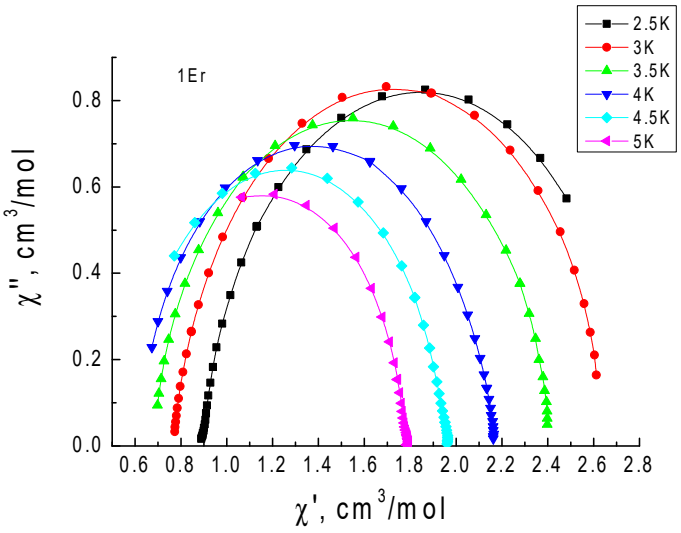

Figure S13. The Cole-Cole plot for **1Er**.

Table S3. The values of the α parameters obtained by approximating the dependences $\chi'(\nu)$ and $\chi''(\nu)$ for the **1Er** complex by the generalized Debye model.

Temperature, K	$\chi'(\nu)$	$\chi''(\nu)$
2.5	0.0924	0.0945
3	0.0768	0.0762
3.5	0.0812	0.0828
4	0.0758	0.0709
4.5	0.0701	0.0544
5	0.0785	0.0528

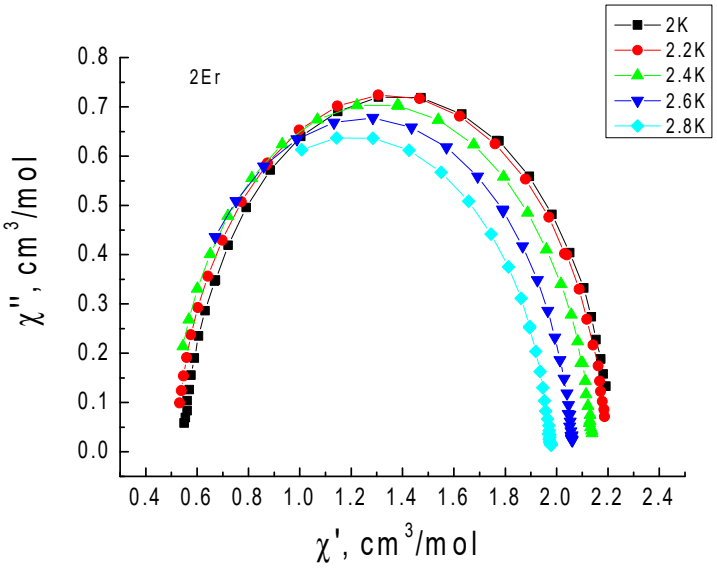

Figure S14. The Cole-Cole plot for **2Er**.

Table S4. The values of the α parameters obtained by approximating the dependences $\chi'(\nu)$ and $\chi''(\nu)$ for the **2Er** complex by the generalized Debye model.

Temperature, K	$\chi'(\nu)$	$\chi''(\nu)$
2	0.0972	0.1159
2.2	0.1007	0.1115
2.4	0.1063	0.1115
2.6	0.1093	0.1146
2.8	0.0924	0.1089

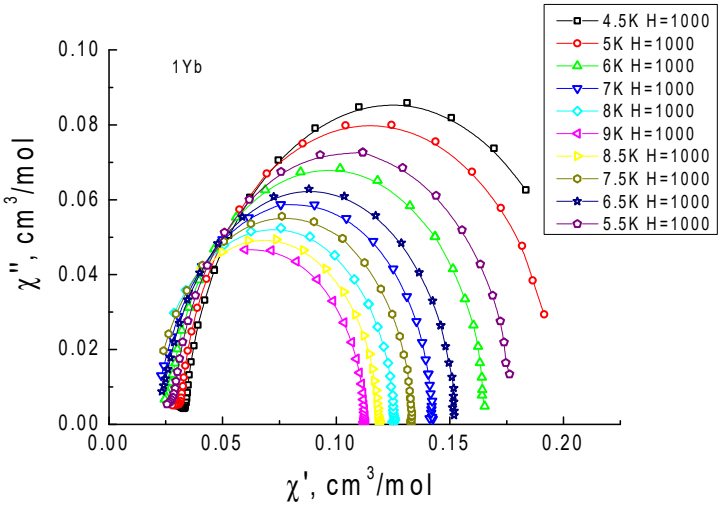

Figure S15. The Cole-Cole plot for **1Yb**.

Table S5. The values of the α parameters obtained by approximating the dependences $\chi'(\nu)$ and $\chi''(\nu)$ for the **1Yb** complex by the generalized Debye model.

Temperature, K	$\chi'(\nu)$	$\chi''(\nu)$
4.5	0.0577	0.0444
5	0.0317	0.0293
5.5	0.0197	0.0224
6	0.0157	0.0198
6.5	0.0148	0.0221

7	0.0088	0.0197
7.5	0.0048	0.0146
8	0.0054	0.0121
8.5	0.0125	0.0096
9	0.0134	0.0147

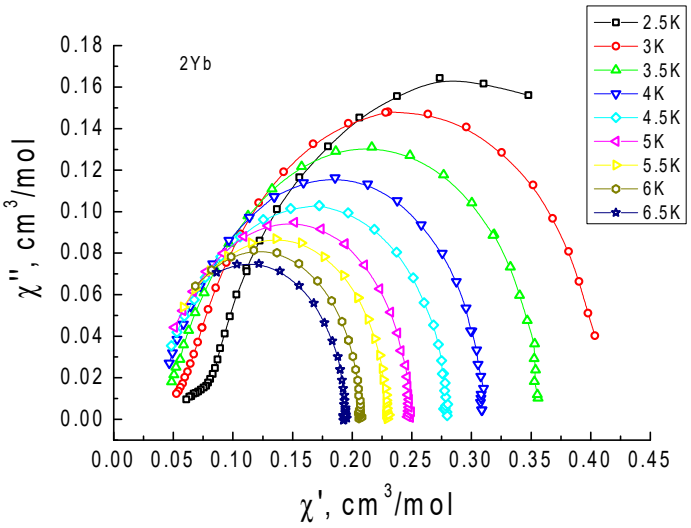

Figure S16. The Cole-Cole plot for **2Yb**.

Table S6. The values of the α parameters obtained by approximating the dependences $\chi'(\nu)$ and $\chi''(\nu)$ for the **2Yb** complex by the generalized Debye model.

Temperature, K	$\chi'(\nu)$	$\chi''(\nu)$
2.5	0.2409	0.2186
3	0.1399	0.1321
3.5	0.0958	0.1004
4	0.0841	0.0972
4.5	0.0700	0.0872
5	0.0519	0.0698
5.5	0.0322	0.0541
6	0.0173	0.0366
6.5	0.0049	0.0259

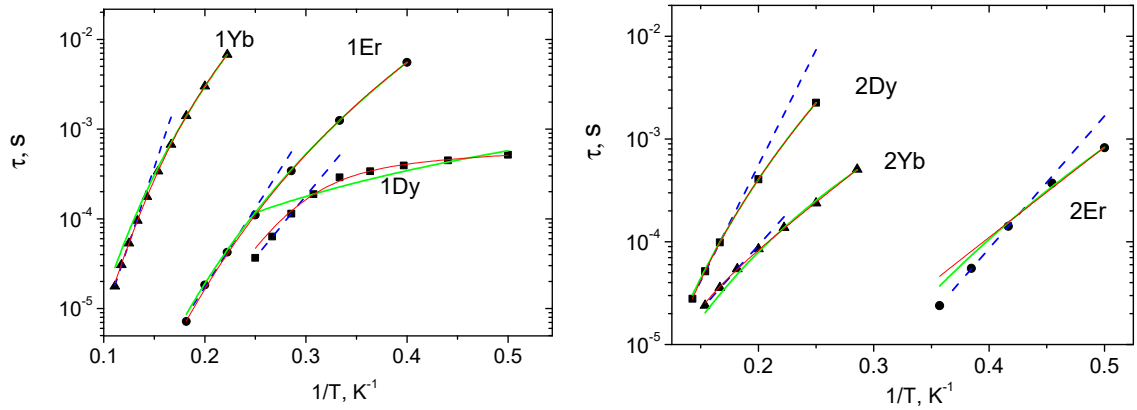

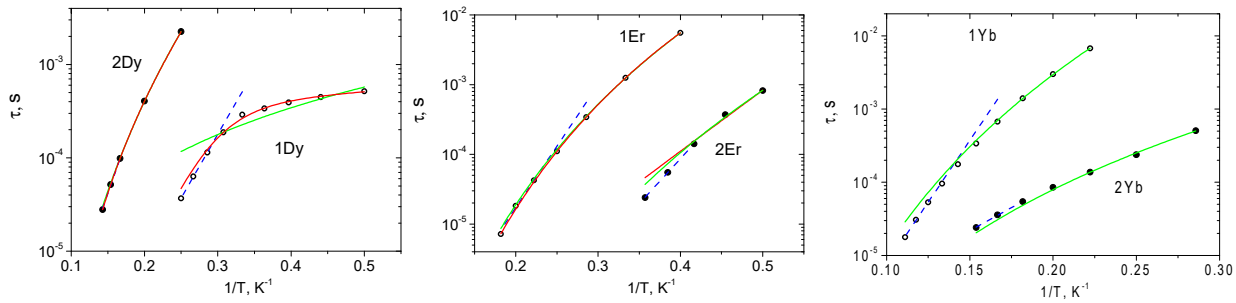

Figure S17. Plots of the τ(1/T) dependences for **1Dy**, **1Er**, **1Yb**, **2Dy**, **2Er**, and **2Yb** in dc-fields of optimal intensity. The blue dotted lines represent the best-fit of experimental data by the Arrhenius equation (Orbach mechanism) at high temperatures. The green solid lines represent the best-fit of experimental data by the Raman relaxation mechanism only. The red solid lines represent the best-fit of experimental data by sum of Raman and Orbach relaxation mechanisms.

Table S7. Parameters of the Orbach relaxation processes for the complexes obtained by approximating the high-temperature part of the temperature dependences of the relaxation time (blue dotted lines on Fig. S17).

Complex	**1Dy**	**1Er**	**1Yb**	**2Dy**	**2Er**	**2Yb**
Field, Oe	1000	1000	1000	1500	1000	1000
T range, K	3.5–4	4.5–5.5	8–9	6–7	3–4	5.5–6.5
U_{eff}/k_B, K	31	40	78	52	30	29
(U_{eff}, cm^{-1})	(22)	(28)	(54)	(36)	(21)	(20)
τ_0, s	1.4×10^{-8}	5.3×10^{-9}	3.2×10^{-9}	1.8×10^{-8}	6.1×10^{-10}	2.9×10^{-7}

Table S8. The *ab initio* computed energy levels (cm^{-1}) with the associated g-tensors of the four lowest KDs for **1Ln** and **2Ln**.

	1Dy				**2Dy**			
KD	***Energy***	g_x	g_y	g_z	***Energy***	g_x	g_y	g_z
1	0.0	0.464	0.894	17.520	0.0	0.240	0.596	17.448
2	54.4	0.503	0.812	13.778	36.2	0.164	0.694	15.111
3	73.8	0.361	0.583	15.197	82.4	3.702	7.031	11.162
4	104.2	0.077	0.959	13.691	96.1	0.781	2.264	13.005

	1Er				**2Er**			
KD	***Energy***	g_x	g_y	g_z	***Energy***	g_x	g_y	g_z
1	0.0	1.324	3.577	13.261	0.0	0.935	3.970	12.087
2	30.0	4.347	4.782	8.309	25.9	0.786	3.009	11.515
3	96.6	0.059	0.875	14.978	51.7	7.680	5.901	3.237
4	135.8	2.490	2.523	9.848	115.7	0.078	1.668	12.427

	1Yb				**2Yb**			
KD	***Energy***	g_x	g_y	g_z	***Energy***	g_x	g_y	g_z
1	0.0	0.355	0.616	7.411	0.0	0.466	1.334	6.638
2	193.2	1.988	2.362	4.766	84.2	0.181	2.107	5.840
3	260.8	3.019	2.705	1.035	277.1	3.335	2.914	1.645
4	354.6	0.574	2.291	6.211	364.8	0.717	1.809	6.617

Table S9. Parameters of the Raman relaxation processes for the complexes obtained by approximating the temperature dependences of the relaxation time (green solid lines on Figure S17).

Complex	1Dy	1Er	1Yb	2Dy	2Er	2Yb
Field, Oe	1000	1000	1000	1500	1000	1000
T range, K	2-4	2.5-5	4.5-9	4-7	2-4	2.5-6.5
C, $K^{-n\_Raman}.s^{-1}$	355.4	0.099	0.001	0.010	2.01	3.03
n_{Raman}	2.3	8.2	7.9	7.7	9.2	5.2

Table S10. Parameters for approximation by the sum Raman and Orbach relaxation processes for the complexes obtained by approximating the temperature dependences of the relaxation time (red solid lines on Figure S17)*.

Complex	1Dy	1Er	1Yb	2Dy	2Er	2Yb
Field, Oe	1000	1000	1000	1500	1000	1000
T range, K	2–4	2.5–5	4.5–9	4–7	2–4	2.5–6.5
C, $K^{-n\_Raman}.s^{-1}$	0.071	0.061	0.002	6.0E−4	0.1	5.6E−4
n_{Raman}	9**	8.6	7.4	9.1	9**	9**
U_{eff}/k_B, K	1.3	9.5	84.5	27.9	20.2	20.3
τ_0, s	2.7×10^{-4}	1×10^{-3}	3.1×10^{-9}	3.6×10^{-6}	3.6×10^{-8}	1.6×10^{-6}

* - for all complexes in the case of approximation by the sum of Raman and Orbach mechanisms, the mutual dependence of parameters was observed.

** - the n_{Raman} was fixed at the specified value, in opposite case it pretend to be more then 10.

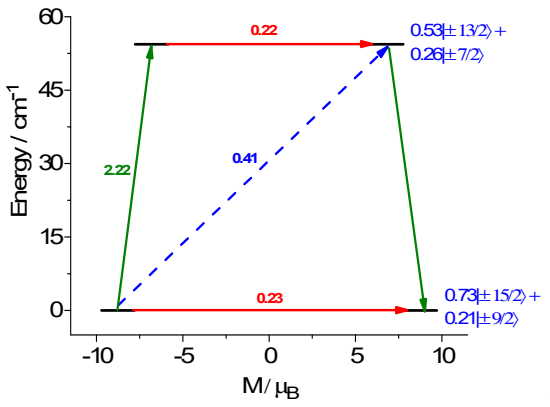

1Dy

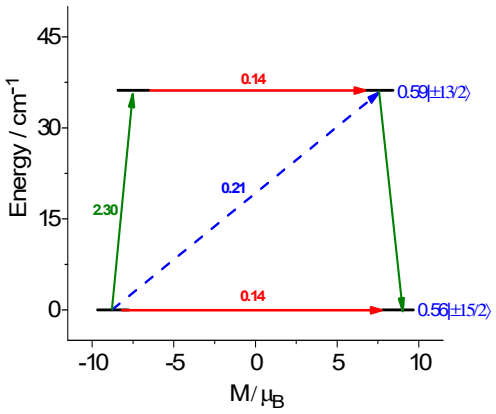

2Dy

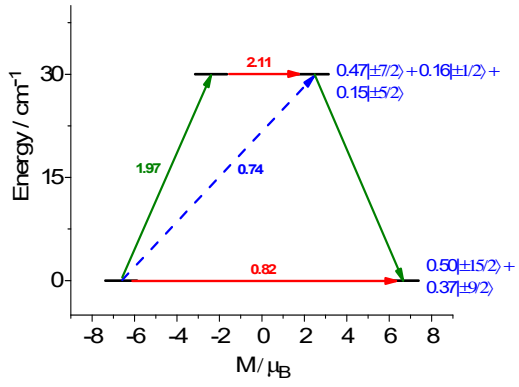

1Er

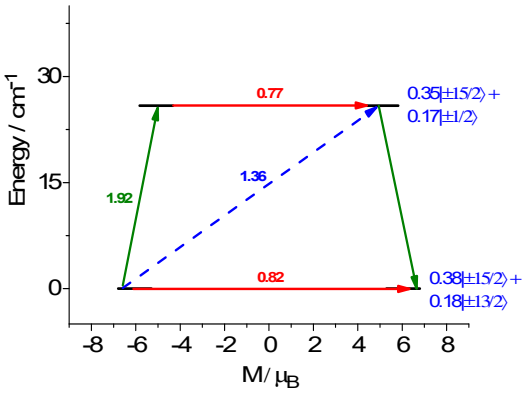

2Er

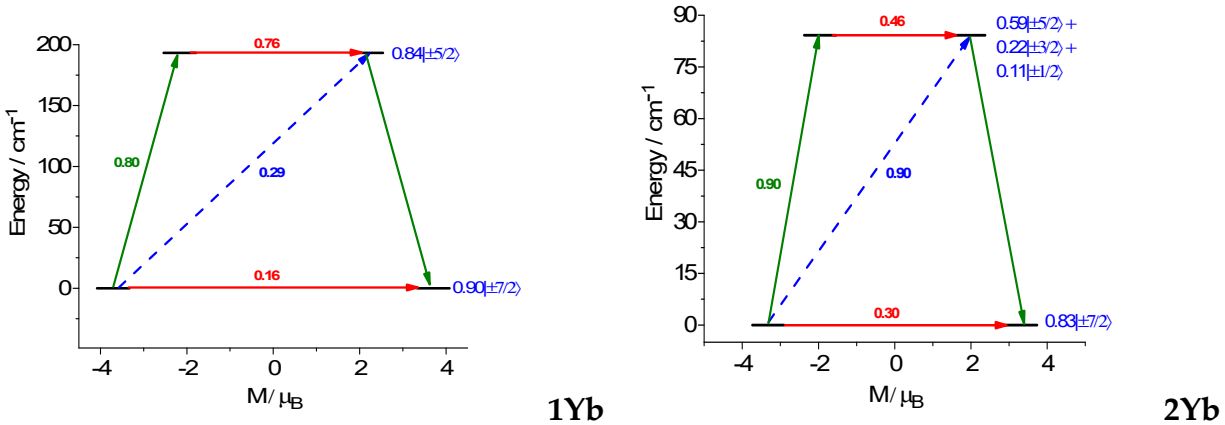

1Yb **2Yb**

Figure S18. Mechanisms of magnetic relaxation of complexes **1Ln** and **2Ln**. The red line indicates the QTM and TA-QTM via ground KD and excited KD respectively. The olive line indicates the transition probability between KD1 and KD2. The blue line indicates mechanism of Orbach relaxation. The blue characters indicate the m_J composition of each KD.

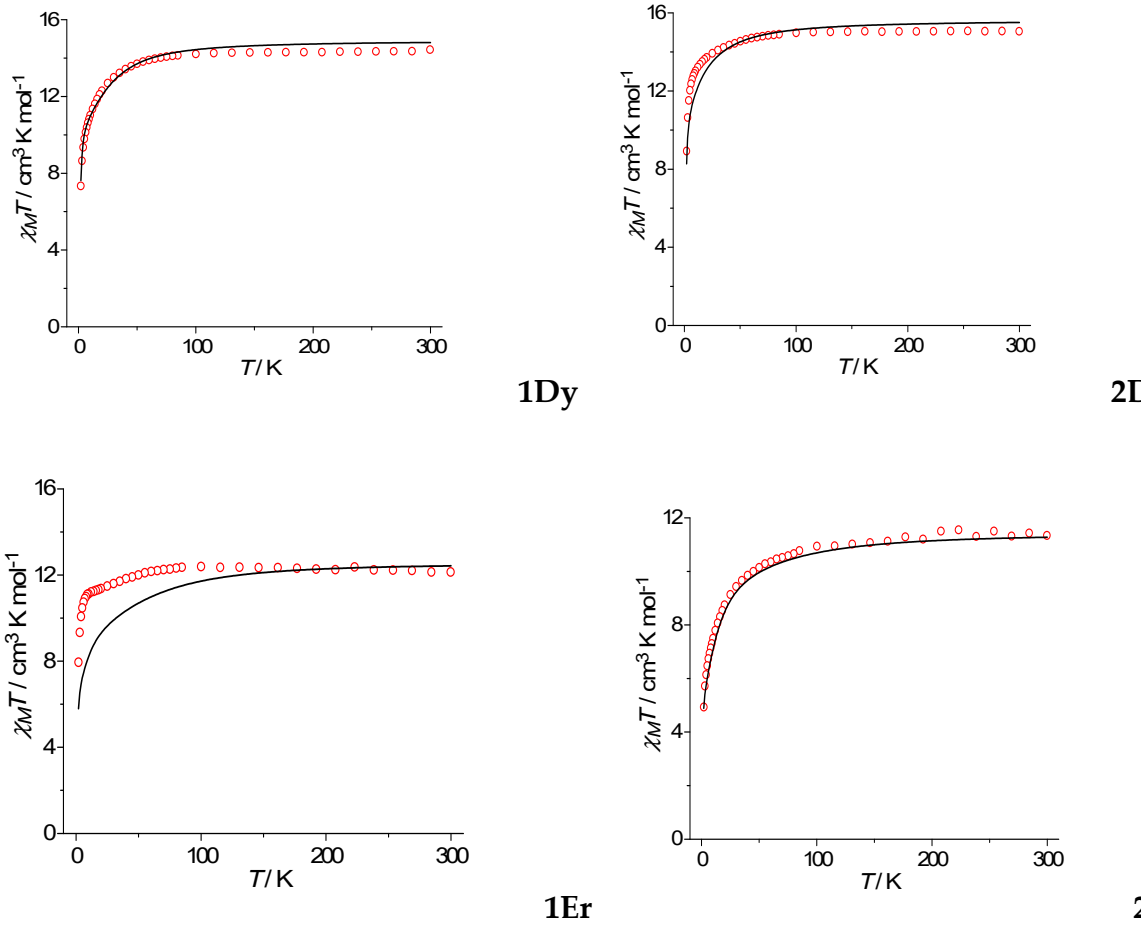

1Dy **2Dy**

1Er **2Er**

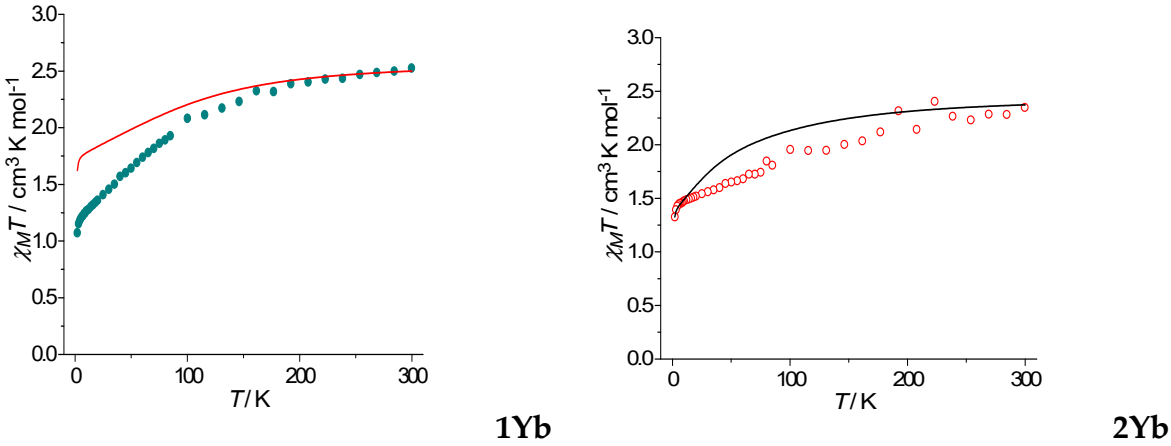

Figure S19. Comparison of the computed magnetic susceptibility of **1Ln** and **2Ln** with experiment. Points correspond to the experimental magnetic susceptibility data. The solid lines are the computed magnetic susceptibilities.

Table S11. Shape Measures calculation for $[Y(H_2O)_6Cl_2]Cl$, isostructural with complexes **1Ln**.

Structure [ML8]	**SAPR-8**	**TDD-8**	**BTPR-8**
	1.103	1.945	2.485

SAPR-8 D4d, Square antiprism
TDD-8 D2d, Triangular dodecahedron
BTPR-8 C2v, Biaugmented trigonal prism

Table S12. Shape Measures calculation for $[Lu(H_2O)_4(terpy)Cl]Cl_2{\cdot}3H_2O$, isostructural with complexes **2Ln**.

Structure [ML8]	**TDD-8**	**JBTPR-8**	**BTPR-8**
YECRIH	1.372	2.776	1.509

TDD-8 D2d, Triangular dodecahedron
JBTPR-8 C2v, Biaugmented trigonal prism J50
BTPR-8 C2v, Biaugmented trigonal prism

Llunell, M.; Casanova, D.; Cirera, J.; Alemany, P.; Alvarez S. ***SHAPE*** *v2.1. Barcelona, Spain, 2013.*

TDD-8

Trapezohedra:
N(2,2A)/O(4,4A), lies exactly in the same plane according to crystallographic symmetry; Cl(2)/N(1)/O(3,5) flat with precision of 0.11 Å
The angle between them is 86°.

BTPR-8

Bases:
N(2)/O(3)O(5), Cl(2)/N(2A)/O(4a)
The angle between them is 172°.
Quadrangular faces
Cl(2)N(2,2A)O(3) 0.15 Å; Cl(2)N(2)O(5,4A) 0.07 Å; O(3,5,4A)/N(2A) 0.08 Å
Caps N(1), O(4)

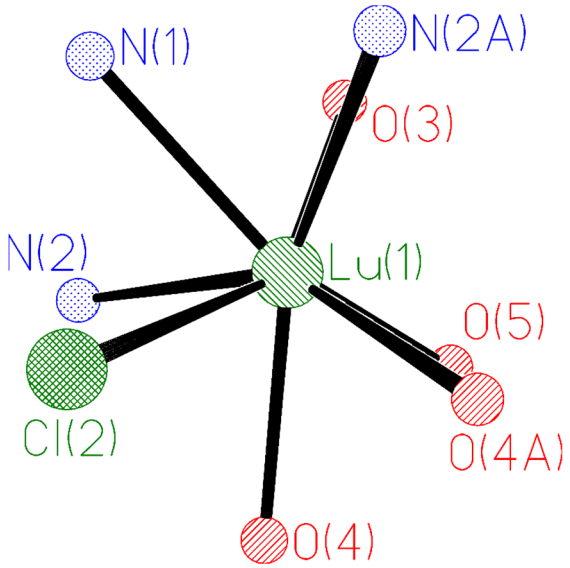

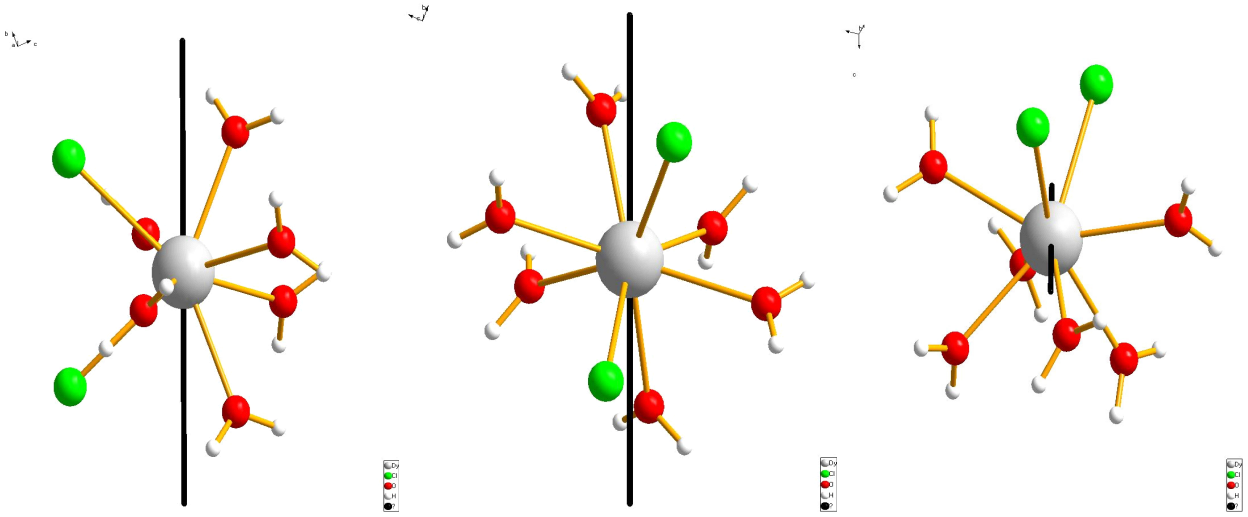

Figure S20. The orientation of the anisotropic axis for the ground state for **1Dy** according to *ab initio* calculations.

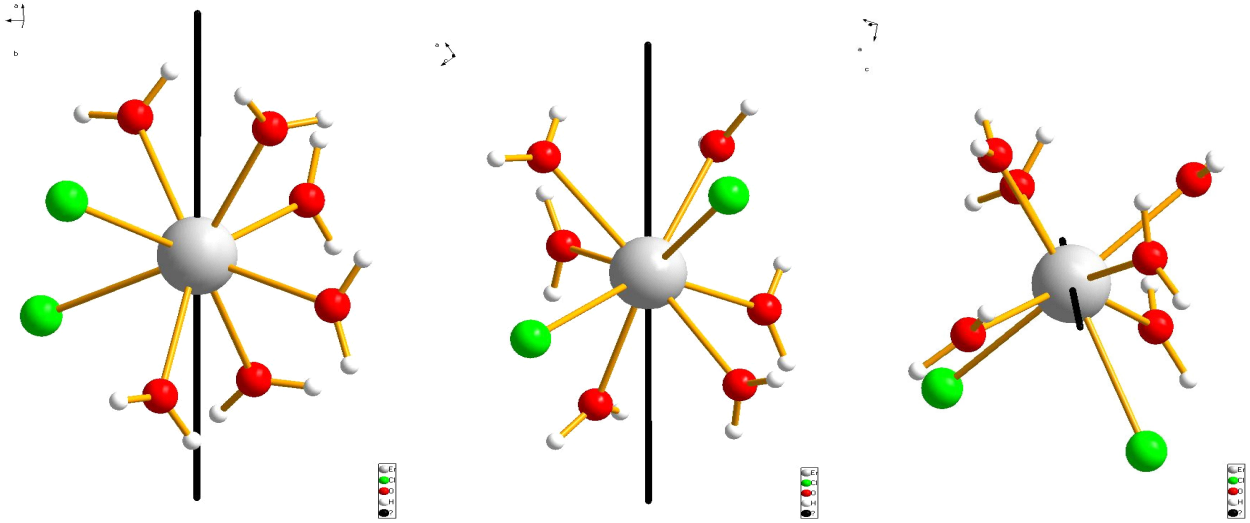

Figure S21. The orientation of the anisotropic axis for the ground state for **1Er** according to *ab initio* calculations.

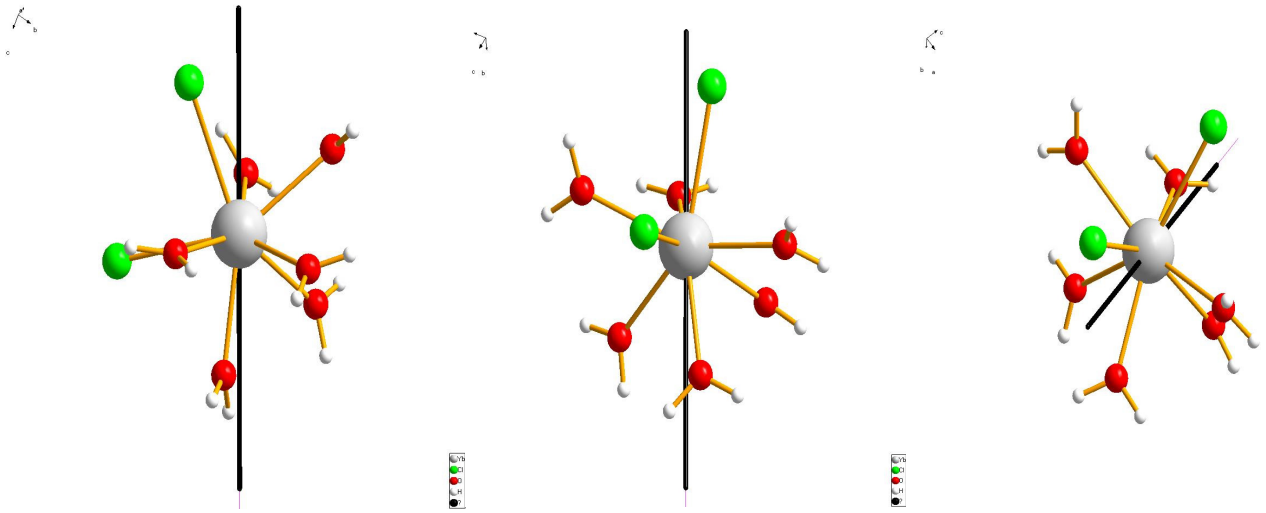

Figure S22. The orientation of the anisotropic axis for the ground state for **1Yb** according to *ab initio* calculations.

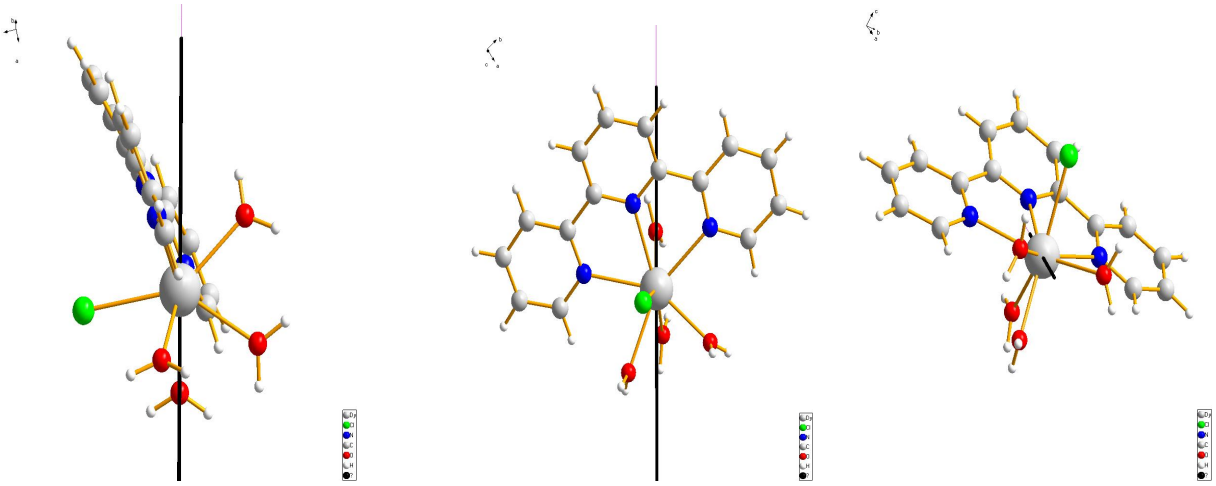

Figure S23. The orientation of the anisotropic axis for the ground state for **2Dy** according to *ab initio* calculations.

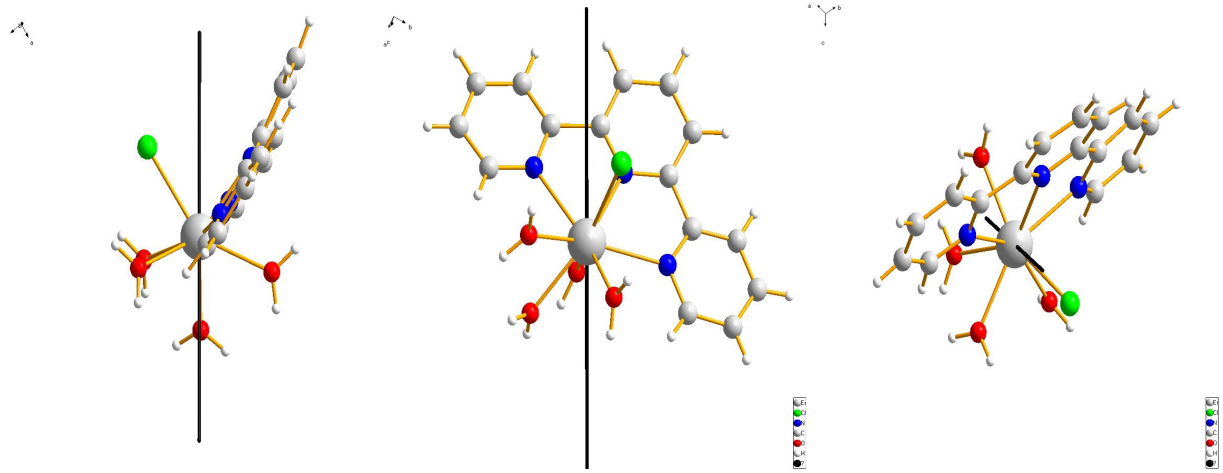

Figure S24. The orientation of the anisotropic axis for the ground state for **2Er** according to *ab initio* calculations.

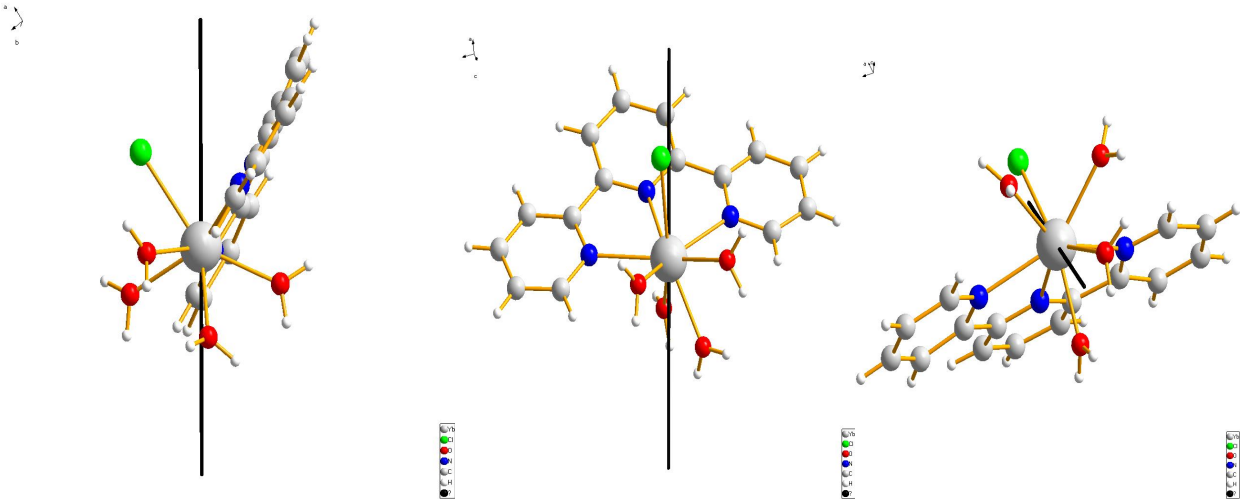

Figure S25. The orientation of the anisotropic axis for the ground state for **2Yb** according to *ab initio* calculations.

Table S13. Calculation of the angles between the magnetic anisotropy axes and the axes of symmetry of the coordination polyhedrons in **1Ln** and **2Ln** complexes.

Complex	*ang1*	*ang2*	*ang3*	*ang4*
1Dy	90.0	71.9		
1Er	90.0	37.3		
1Yb	60.0	72.8		
2Dy			75.1	80.1
2Er			59.2	44.5
2Yb			76.5	37.9

Complexes **1Ln** and **2Ln** occupy special positions in the structures and are located on the twofold axis and the *m* plane, respectively. A natural description of the location of the magnetic anisotropy axis is the angle between it and the symmetry elements of the complexes. In addition, one should consider the mutual arrangement of the magnetic anisotropy axis and Cl atoms, the only charged ligands in the complexes. For the complexes **1Ln**, we calculated the angle between the magnetic anisotropy axis and the twofold axis (*ang1*), as well as the angle between the magnetic anisotropy axis and the Cl, Cl′, Ln plane (*ang2*). For the complexes **2Ln**, the angle between the magnetic anisotropy axis and the *m* plane (*ang3*), as well as the angle between the magnetic anisotropy axis and the Ln-Cl segment (*ang4*), were calculated.